Peer-reviewed version available at Metals 2018, 8, 371; doi:10.3390/met8050371

Article

Fabrication technology and material characterization of hot rolled cylindrical Fe-6.5wt.% Si bars

Shibo Wen, Shaowei Xue, Chaoyu Han, Binbin Liu, Yongfeng Liang and Feng Ye*

State Key Laboratory for Advanced Metals and Materials, University of Science and Technology Beijing, Beijing, 100083, China; wenshibo10@126.com (S. B. Wen); qierwangzi@126.com (S.W. Xue); ihancy@hotmail.com (C. Y. Han); bbliu@ustb.edu.cn (B.B. Liu); liangyf@skl.ustb.edu.cn (Y. F. Liang); yefeng@skl.ustb.edu.cn (F. Ye)

* Correspondence: yefeng@skl.ustb.edu.cn; Tel.: +86-10-6233-3899

Abstract: Cylindrical Fe-6.5wt.% Si bars with 7.5 mm in diameter were successfully fabricated from as cast ingot through three rolling stages within 10 passes: rough rolling at 850–900 °C and 8–10 m/min, medium rolling at 800–850 °C and 10–15 m/min, and finish rolling at 800–850 °C and 12–18 m/min. The evolution of microstructure, texture and ordered structure, and the mechanical property are investigated. The results showed that the grains were refined by the hot bar rolling. Area fractions of the {100}<011> oriented grains and the {011}<100> oriented grains decreased to 0 during the hot bar rolling. Whereas, the {100}<001> component, the {011}<211> component and the {112}<110> component increased, and γ fiber with {111}<110> component was dominant. DO_3 ordered phase were suppressed, and B2 ordered domains were refined after the hot bar rolling. Ductility of the as rolled bar was higher than that of the rotary swaged bar, due to the absence of the DO_3 ordered phase and the fine grains in the rolled bar. Hence, the hot bar rolling technology is an excellent process to fabricate the Fe-6.5wt.% Si bars.

Keywords: Fe-6.5wt.% Si alloy; hot bar rolling; microstructure; texture; mechanical property

1. Introduction

Fe-6.5wt.% Si alloy has excellent soft magnetic properties such as high electrical resistance, high relative permeability, nearly zero magnetostriction, low coercive force, and low iron loss, which make this alloy promising in high frequency fields, such as transformers, power generators and electric relay [1, 2]. However, it is very brittle at room temperature because of ordered structures such as B2 ($Pm\bar{3}m$) and DO_3 ($Fm\bar{3}m$) forming in this alloy [3, 4]. Various techniques have been developed to produce plates to avoid the room-temperature embrittlement, e.g., chemical vapor deposition [5], hot dipping [6], spray forming [7-9], rapid solidification [10-12], direct powder rolling [13]. Moreover, a hot-warm-cold rolling method combined with proper heat treatments was reported to fabricate the sheets of thickness 0.03–0.05 mm [14-16].

Recent patents [17] revealed that transformers can be constructed by coiling silicon steel wires on a copper conductor. This suggests that the high silicon steel wires with outstanding soft magnetic properties can be a good choice for industry application. Previously, Fe-6.5wt.% Si wires with diameter of 1.6 mm were prepared through die forging, hot rotary swaging, and hot drawing process [18]. However, the coarse and inhomogeneous grains, and the poor surface quality of the rotary swaging bars result in the low productivity of wires. This hinders the production of the Fe-6.5wt.% Si wires. These problems mentioned above can be solved by bar rolling [19]. In fact, rolling is an efficient way to produce bars and wires from as cast ingots. Because the Fe-6.5wt.% Si alloy exhibited low formability in sheet rolling [20], systematic research on optimizing microstructure, surface quality and mechanical property need to be carried out to improve the bar productivity.

Preprints (www.preprints.org) | NOT PEER-REVIEWED | Posted: 29 March 2018 doi:10.20944/preprints201803.0246.v1

Peer-reviewed version available at Metals 2018, 8, 371; doi:10.3390/met8050371

Recently, a lot of researches [21, 22] involve the texture evolution of rolling process of the Fe-6.5wt.% Si sheets. However, there are few reports on bar rolling. The bar rolling technology differs greatly from the sheet rolling technology in temperature, rolling force and rolling torque. Hence, it is also necessary to investigate the texture evolution during hot bar rolling.

In this paper, a series appropriate parameters for hot bar rolling the Fe-6.5wt.% Si alloy were determined. The evolution of microstructure, texture and ordered structure were investigated, and the mechanical property of the Fe-6.5wt.% Si bars was studied to obtain the excellent mechanical property to improve the drawing efficiency of the Fe-6.5wt.% Si wires.

2. Materials and Methods

2.1. Starting materials

Fe-6.5wt.% Si alloy ingots were prepared by melting pure iron (99.5wt.%) and metallic silicon (99wt.%) in vacuum through induction heating. Figure 1 shows a process flow chart of various shapes of the starting Fe-6.5wt.% Si alloy. The ingots were forged into square billets (cross section of 24×24 mm²) and rods (diameter of Φ13 mm) at 800–1100 °C. Subsequently, the as forged rods were hot rotary swaged into thin bars (diameter of Φ6 mm) at 850–950 °C. The chemical composition is listed in Table 1.

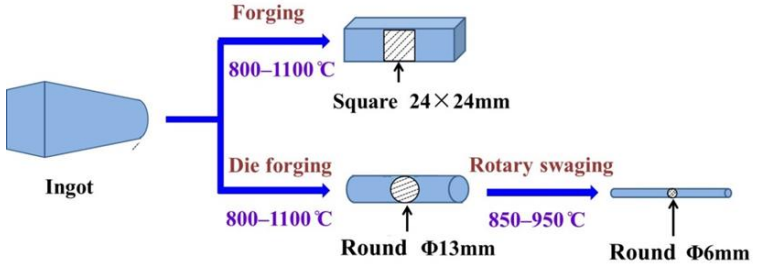

Figure 1. Process flow chart of various shapes of the Fe-6.5wt.% Si alloy.

Table 1. Chemical composition of Fe-6.5wt.% Si alloy (wt.%).

C	Si	Mn	S	P	Ti	B	Fe
0.009	6.510	0.015	0.0009	0.054	0.005	0.0004	Bal

2.2. Rolling equipment

Fe-6.5wt.% Si bars were prepared by Φ 120 Hot Rolling Mill. The Fe-6.5wt.% Si alloy were heated by WX3–75–9 Heat-treatment Furnace (Dotrust Exact Science, Beijing, China).

2.3. Microstructures and mechanical properties characterization

Specimens of the Fe-6.5wt.% Si bars were polished and etched with a solution of 5% HNO_3 in deionized water. Microstructures were observed by an optical microscope (Zeiss, Jena, Germany). Micro-hardness of the corresponding sample was examined by 402MVD micro-hardness indenter (Wolpert Wilson Instruments, Shanghai, China).

Texture of the specimen was detected by Electron backscattered diffraction (EBSD) detector mounted on the ZEISS SUPRA 55 scanning electron microscope (Oxford Instruments, Oxford, UK). HKL Channel 5 programs were used for processing the datum such as orientation distribution functions (ODFs) and texture components of the specimens with a deviation of 15°.

Ordered structures during the hot bar rolling were investigated by Tecnai G² F30 transmission electron microscopy (TEM) (Thermo Fisher Scientific Inc., Hillsboro, USA). The specimens were made by electropolishing in a solution of 5% perchloric acid and 95% ethanol at a voltage of 30 V at -20 °C.

Preprints (www.preprints.org) | NOT PEER-REVIEWED | Posted: 29 March 2018 doi:10.20944/preprints201803.0246.v1

Peer-reviewed version available at Metals 2018, 8, 371; doi:10.3390/met8050371

Tensile ductility of the Fe-6.5wt.% Si bar was measured by DDL50 high temperature electronic universal testing machine (Sinotest Equipment Co., ltd., Jilin, China). The tensile tests were carried out at strain rate of 5×10^{-4} s^{-1} and at temperature ranging of 600–800 °C

3. Fabrication of Fe-6.5wt.% Si bars by hot bar rolling technique

Rolling temperature, rolling pass, and rolling groove are major parameters in the shape rolling design process [23, 24]. The design of these parameters referred to the achievement of predecessors [19, 25]. Figure 2 shows a process flow chart of hot bar rolling for the Fe-6.5wt.% Si alloy.

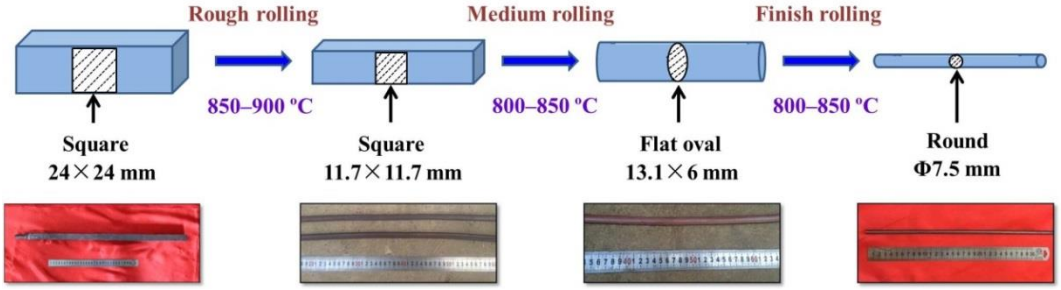

Figure 2. Process flow chart of hot bar rolling for the Fe-6.5wt.% Si alloy.

3.1. Rolling temperature and rolling pass

The rolling temperature depends on the high-temperature mechanical property of the Fe-6.5wt.% Si alloy. The rolling pass can be calculated, according to the shape and size of the forging and the bar. Φ7.5 mm bars were prepared through three rolling stages with 10 passes: rough rolling at 850–900 °C and 8–10 m/min, medium rolling at 800–850 °C and 10–15 m/min, and finish rolling at 800–850 °C and 12–18 m/min.

3.2. Rolling groove and deformation ratio

The rolling grooves are determined by the deformation ratio and the flow stress. The hot bar rolling parameters including rolling pass, groove system, and deformation ratio are listed in Table 2. The hexagon-square-oval-square sequence was used as the rough rolling stage to obtain rapid reduction of sectional area. According to our previous study [26], a 50%-deformation was chosen in order to obtain stable and secure microstructure transformation, and improve the workability. The oval-square-oval-round sequence and the medium deformation ratio of 30% were designed as the medium rolling parameters to improve surface quality. The oval-round sequence and the 15%-deformation were used to achieve exact dimensions during the finish rolling.

Table 2. Chemical composition of Fe-6.5wt.% Si alloy (wt.%).

Rolling stage	Pass	Groove	Area (mm^2)	Elongation coefficient	Deformation ratio
–	0	Square -	S_0=576.0	–	–
Rough rolling	1	Hexagon	S_1=409.5	μ_1= S_0/ S_1=1.41	L_0/ L_1=41%
	2	Square	S_2=269.0	μ_2= S_1/ S_2=1.52	L_1/ L_3=52%
	3	Flat oval	S_3=182.8	μ_3= S_2/ S_3=1.47	L_2/ L_3=47%
	4	Square	S_4=136.9	μ_4= S_3/ S_4=1.33	L_3/ L_4=33%
Medium rolling	5	Flat oval	S_5=102.6	μ_5= S_4/ S_5=1.33	L_4/ L_5=33%
	6	Square	S_6=81	μ_6= S_5/ S_6=1.27	L_5/ L_6=27%
	7	Flat oval	S_7=64.5	μ_7= S_6/ S_7=1.26	L_6/ L_7=26%
	8	Round	S_8=56.7	μ_8= S_7/ S_8=1.14	L_7/ L_8=14%
Finish rolling	9	Flat oval	S_9=49.1	μ_9= S_8/ S_9=1.15	L_8/ L_9=15%
	10	Round	S_{10}=44.2	μ_{10}= S_9/ S10=1.11	L_9/ L_{10}=11%

3.3. Rolling gap

The rolling gap also influences the rolling stability and the shape of materials. In the rough rolling stage and the medium rolling stage, the rolling gap was adjustable, and the profile geometry was variable, which were conducive to reducing the risk of metal twisting. At the stage of the finish rolling, the rolling gap decreased to 0 to ensure the shape and the surface quality.

4. Results and Discussion

4.1. Microstructure evolution

Figure 3 shows microstructures of the as forged Fe-6.5wt.% Si alloy along radial direction (RD) and axial direction (AD). The coarse grains were inhomogeneous, and the grain sizes along RD and AD were similar before the hot bar rolling, as shown in Figure 3a and 3b. It indicates a full recrystallization and grain growth due to the long tempering time during the forging.

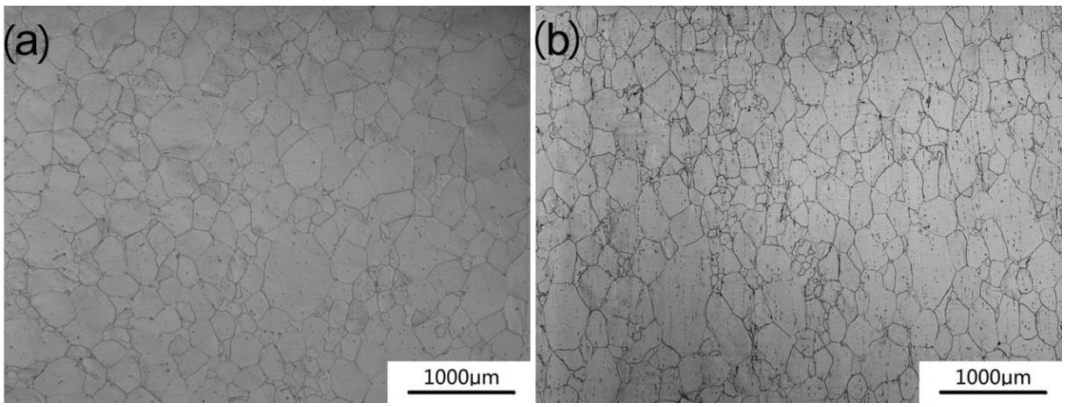

Figure 3. Microstructures of the as forged Fe-6.5wt.% Si alloy along (a) radial direction and (b) axial direction.

Figure 4 shows microstructure evolution of the Fe-6.5wt.% Si alloy along RD during various rolling passes. The coarse and inhomogeneous grains were refined, and the grain size decreased with the increase of the total deformation. The small deformation along RD and the high rolling temperature (> 800 °C) result in the appearance of the dynamic recrystallization [27], which lead to the grains refining.

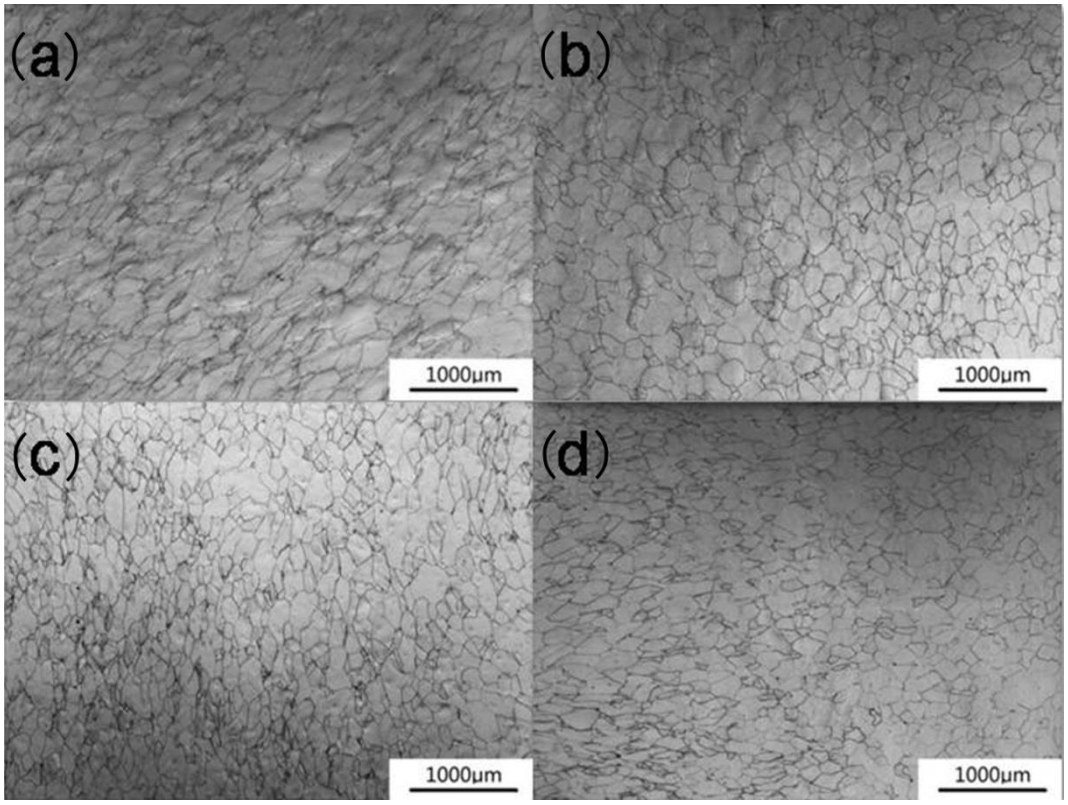

Figure 4. Microstructure evolution of the Fe-6.5wt.% Si alloy along radial direction during various rolling passes: (a) the 4th pass; (b) the 6th pass; (c) the 8th pass; (d) the 10th pass.

Figure 5 shows the microstructure evolution of the Fe-6.5wt.% Si alloy along AD during various rolling passes. The coarse grains were deformed and elongated along AD after the rough rolling, as shown in Figure 5a. At the stage of medium rolling, the elongated grains at the edge were recrystallized, whereas the deformed grains kept elongated at the center, as represented in Figure 5b and 5c. It indicates that dynamic recrystallization occurs at the edge, owing to the large deformation. However, the small deformation cannot meet the conditions of the dynamic recrystallization, and the recrystallization will not occur at the center. In the finish rolling stage, the equiaxed grains instead of the elongated grains existed in the Φ7.5 mm bars due to the full dynamic recrystallization, as shown in Figure 5d.

Preprints (www.preprints.org) | NOT PEER-REVIEWED | Posted: 29 March 2018 doi:10.20944/preprints201803.0246.v1

Peer-reviewed version available at Metals 2018, 8, 371; doi:10.3390/met8050371

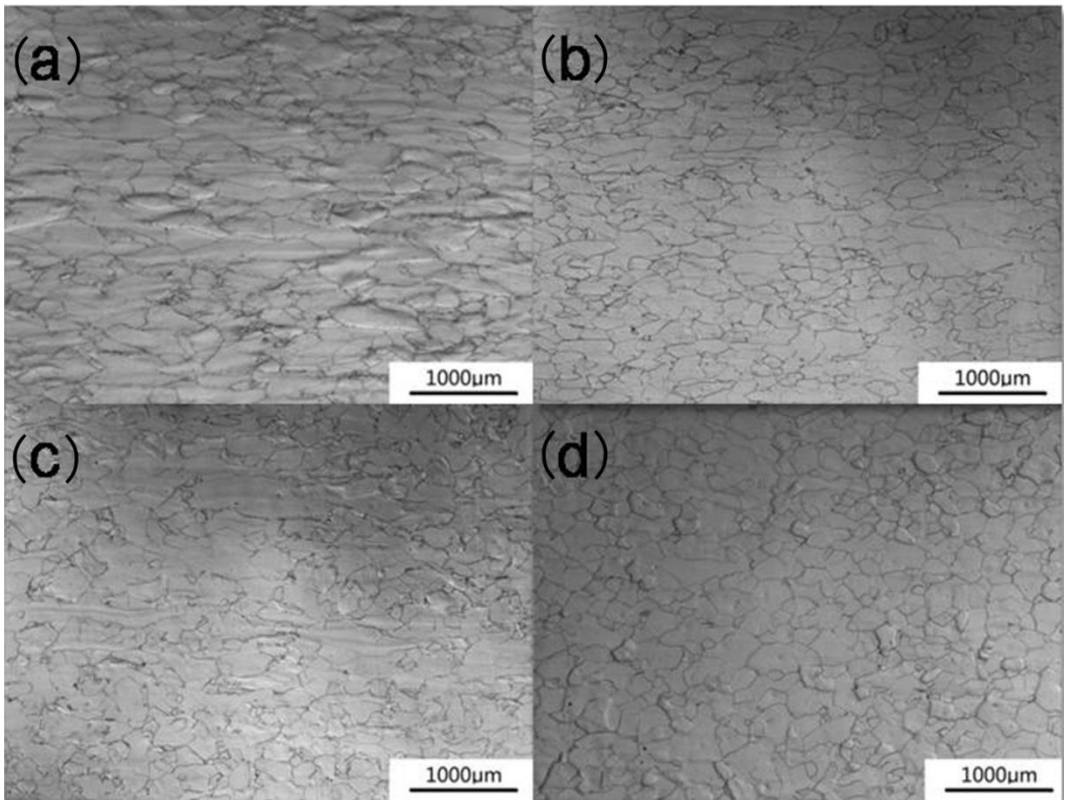

Figure 5. Microstructure evolution of the Fe-6.5wt.% Si alloy along axial direction during various rolling passes: (a) the 4th pass; (b) the 6th pass; (c) the 8th pass; (d) the 10th pass.

Figure 6 shows the variations of the grain sizes and the micro-hardness during the hot bar rolling. It was observed that the grains were refined, with the size decreasing from 285 to 98 μm along RD, and from 300 to 108 μm along AD, as represented in Figure 6a. The micro-hardness along both RD and AD decreased slightly from 400 HV during the bar rolling, and then increased to 400 HV, as shown in Figure 6b. Specially, the value (AD micro-hardness – RD micro-hardness) increased from 3 HV to 17 HV, and then decreased to 3 HV.

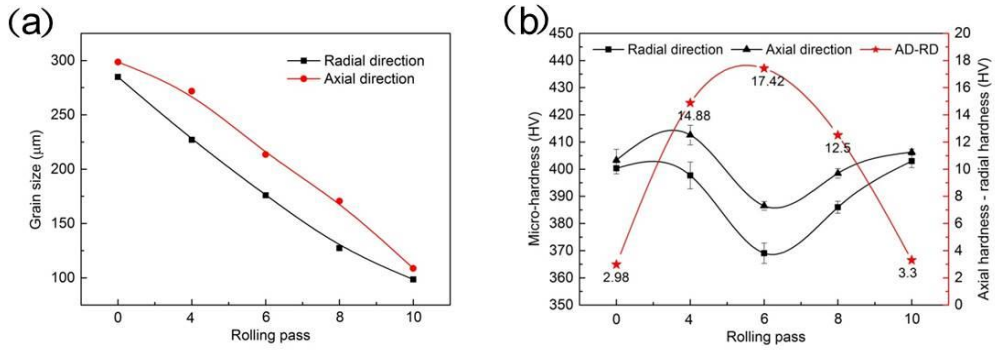

Figure 6. Variations of (a) the grain sizes and (b) the micro-hardness of the Fe-6.5wt.% Si alloy during the hot bar rolling.

4.2. Texture evolution

Figure 7 shows the φ2 = 0° and φ2 = 45° ODF sections of the Fe-6.5wt.% Si alloy during the hot bar rolling. Figure 8 summarizes the typical texture components with a deviation of 15°. Combining

Preprints (www.preprints.org) | NOT PEER-REVIEWED | Posted: 29 March 2018 doi:10.20944/preprints201803.0246.v1

Peer-reviewed version available at Metals 2018, 8, 371; doi:10.3390/met8050371

Figure 7a and 8a, the sample exhibited α fiber with {100}<011> component (Rotation–cube texture), γ fiber with {111}<110> component, and η fiber with {011}<100> component (Goss texture) after the rough rolling (the 4th pass). Furthermore, the area fractions of α oriented grains, γ oriented grains, and η oriented grains were 15.7%, 22.8% and 17.7%, respectively, as shown in Figure 8a.

After the medium rolling (the 8th pass), the most striking feature of the texture was that γ fiber was the dominant component with a peak at {111}<110>, as shown in Figure 7b. There also existed other textures such as α fiber with weak {100}<011> component, and η fiber with weak {100}<001> component (Cube texture). The area fractions of α oriented grains, γ oriented grains, and η oriented grains were 8.7%, 35.9% and 10.0%, respectively, as shown in Figure 8b.

Various kinds of textures existed in the finished rolling specimen (the 10th pass), such as α fiber with {112}<110> component, γ fiber with {111}<110> component, η fiber with {100}<001> component, and weak {011}<211> component (Brass texture), as represented in Figure 7c. It was observed that the area fractions of these textures were 14.5%, 12.7%, 9.2% and 7.5% in sequence.

According to the cubic crystal symmetry and the nearly orthotropic symmetry of the hot bar rolling specimens, α fiber, γ fiber, and η fiber are the most relevant deformation textures for bcc metals during hot rolling [28, 29]. In addition, slip occurs along <111>–type directions within the {110} planes during deformation, and the grain orientation evolves the {100}<011> orientation. Finally, the {100}<011> orientation of the grains rotates to the {112}<110> orientation [29]. Hence, the fractions of the {100}<011> component decreases, and that of the {112}<110> component increases. The high rolling temperature and low deformation ratio results in the full recrystallization and the grain growth for the Fe-6.5wt.%Si alloy in the finish rolling stage, which makes the γ fiber slightly weaken [30, 31].

From the above indications, the area fractions of the {100}<011> oriented grains and the {011}<100> oriented grains decrease to 0%, however, the area fractions of the {100}<001> component, the {011}<211> component and the {112}<110> component increase during the rolling. Notably, γ fiber with {111}<110> component is dominant during the hot bar rolling.

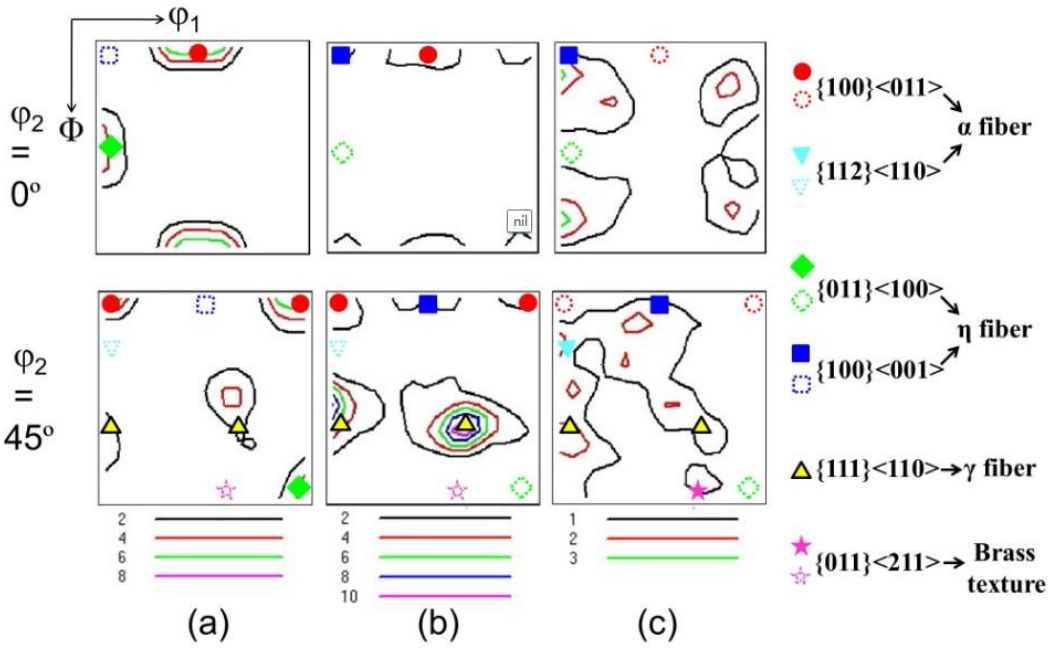

Figure 7. φ2 = 0° and φ2 = 45° ODF sections of the Fe-6.5wt.% Si alloy during hot bar rolling: (a) rough rolling; (b) medium rolling; (c) finish rolling.

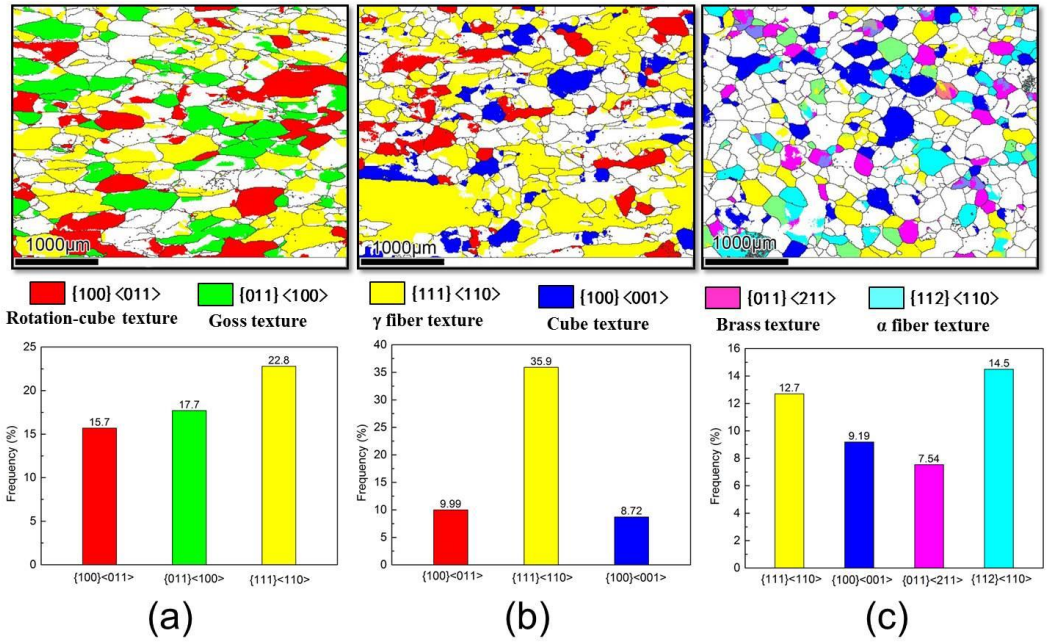

Figure 8. Texture components of the Fe-6.5wt.% Si alloy with a deviation of 15° during hot bar rolling: (a) rough rolling; (b) medium rolling; (c) finish rolling.

4.3. Ordered structure evolution

Figure 9 shows the diffraction patterns with [011] zone axes and the dark field image for B2 and DO_3 in the as forged Fe-6.5wt.%Si alloy. The diffraction pattern indicates that there exist B2 and DO_3 ordered phases in the as forged sample, as represented in Figure 9a. The B2 domains and the DO_3 domains were visible in the dark field image using the (200) superlattice diffraction spot, and the (111) superlattice diffraction spot, respectively [32-34]. The size of the coarse B2 domains was 300–500 nm, and the fine DO_3 ordered domains with 20–40 nm were observed, as shown in Figure 9b and 9c. Furthermore, smoothly curved a′/4 <111> anti-phase boundary (APB) was clearly observed in the Figure 9b [35].

Preprints (www.preprints.org) | NOT PEER-REVIEWED | Posted: 29 March 2018 doi:10.20944/preprints201803.0246.v1

Peer-reviewed version available at Metals 2018, 8, 371; doi:10.3390/met8050371

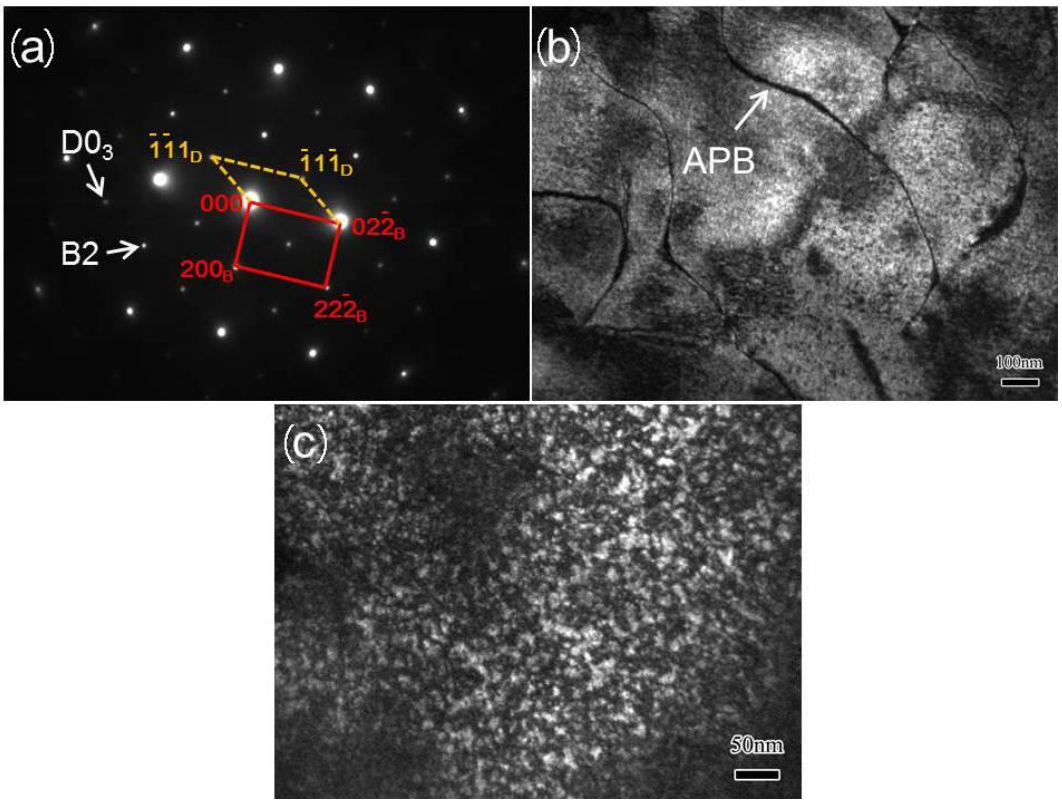

Figure 9. TEM micrograph of the as forged Fe-6.5wt.% Si alloy: (a) diffraction patterns with [011] zone axes; (b) dark field image for B2 using (200) diffraction spot; (c) dark field image for DO_3 using (111) diffraction spot.

Figure 10 shows the diffraction patterns with [011] zone axes and the dark field image for B2 in the rolled bar. Only the B2 diffraction spots were observed in the diffraction patterns. The characteristic diffraction spots of the DO_3 ordered phases became so weak that its dark field image could not be obtained, as shown in Figure 10a. Moreover, the B2 ordered domains were refined, and its size was 40–80 nm, as represented in Figure 10b. It indicates that the degree of order decreases after the hot bar rolling.

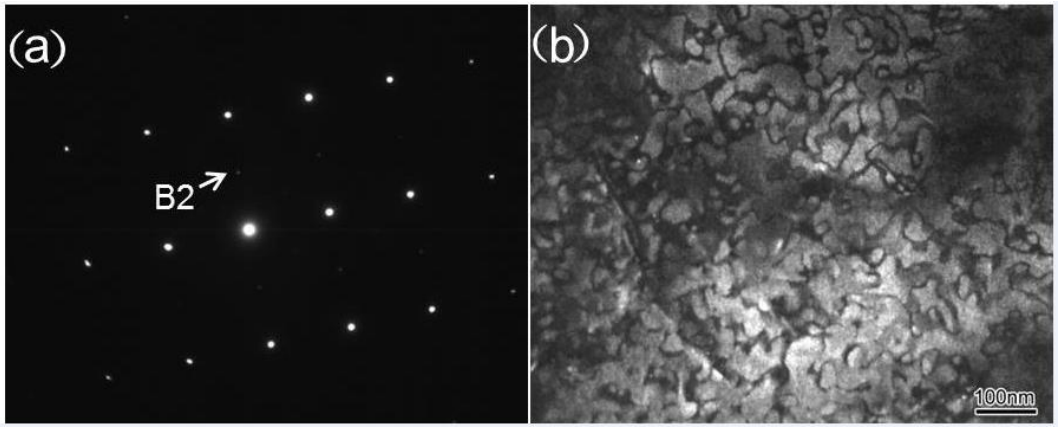

Figure 10. TEM micrograph of the Fe-6.5wt.% Si alloy after finish rolling: (a) diffraction patterns with [011] zone axes; (b) dark field image for B2 using (200) diffraction spot.

Preprints (www.preprints.org) | NOT PEER-REVIEWED | Posted: 29 March 2018 doi:10.20944/preprints201803.0246.v1

Peer-reviewed version available at Metals 2018, 8, 371; doi:10.3390/met8050371

4.4. Mechanical property

Figure 11 shows the stress-strain curves for both the rotary swaged and hot rolled bars of Fe-6.5wt.% Si alloy at a strain rate of 5×10^{-4} s^{-1} and temperatures of 600–800 °C. The corresponding elongations and yield stresses are represented in Figure 12. The stress rarely increased with the strain after the yielding during the tension in all stress-strain curves (Figure 11). The elongation and the yield stress of the rotary swaged and hot rolled bars were similar at 600 °C, the values of which were almost 40 % and 320 MPa, respectively.

At 700 °C, the stress remained constant (rotary swaging: 140 MPa, hot bar rolling: 125MPa) after the yielding (rotary swaging: 136 MPa, hot bar rolling: 120MPa). Similarly, the stress of the rotary swaged sample maintained the value of 30 MPa at 800 °C, and the stress of the hot bar rolled specimen kept a constant value of 21 MPa (Figure 11). These indicate that the dynamic softening offsets the work hardening, and, consequently, the stress remains stable during the tension at 700–800 °C. Generally, as the deformation progresses, the dislocation proliferation takes place, and it subsequently leads to the increase of dislocation density. This results in the work hardening. However, due to the high temperature during the deformation, the dislocations cross slip and climb easily for high stacking fault energy materials such as the Fe-6.5wt.% Si alloy, which can reduce the dislocation density, namely, the dynamic recovery occurs. All of these lead to the dynamic softening offsets the work hardening [36]. Hence, the stress remains stable during the tension at 700–800 °C.

The yield stress of the rotary swaged and hot rolled bars were similar, with the values of 130 MPa (at 700 °C) and 20 MPa (800 °C), respectively. However, the elongation of the rotary swaged specimen was lower than that of the hot bar rolled sample at 700–800 °C, as shown in Figure 12a. Yang et al. [37] fabricated non-oriented Fe-6.5wt.% Si bars by hot rotary swaging, and the size of the coarse grain reached 800 μm. Coarse B2 ordered phase (500–1000 nm) and DO_3 ordered phase (40–80 nm) existed in the sample. More importantly, the DO_3 ordered phase and the coarse grain make the ductility reduce [38]. Although most of the grains in the as rolled bars are no orientation, fine grains are obtained, especially, the DO_3 ordered phase is suppressed. All of the factors result in higher ductility of the hot bar rolled specimen than that of the rotary swaged sample. Thus, the hot bar rolling is the better way to fabricate the Fe-6.5wt.% Si bars, compared with the rotary swaging.

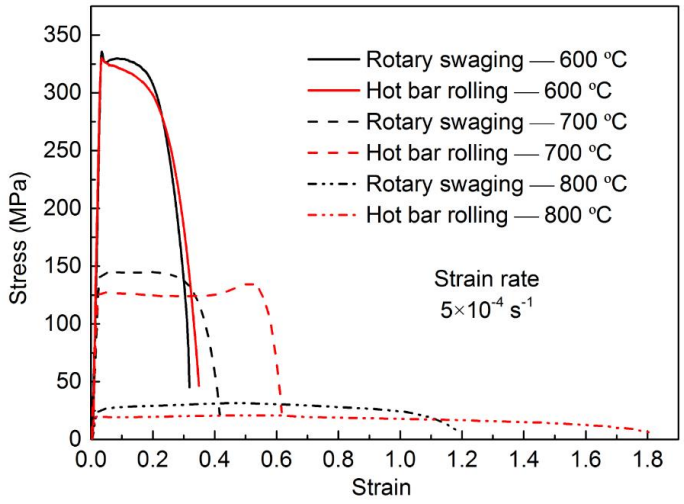

Figure 11. Stress-strain curves for both the rotary swaged and hot rolled bars of Fe-6.5wt.% Si alloy at various tensile temperatures.

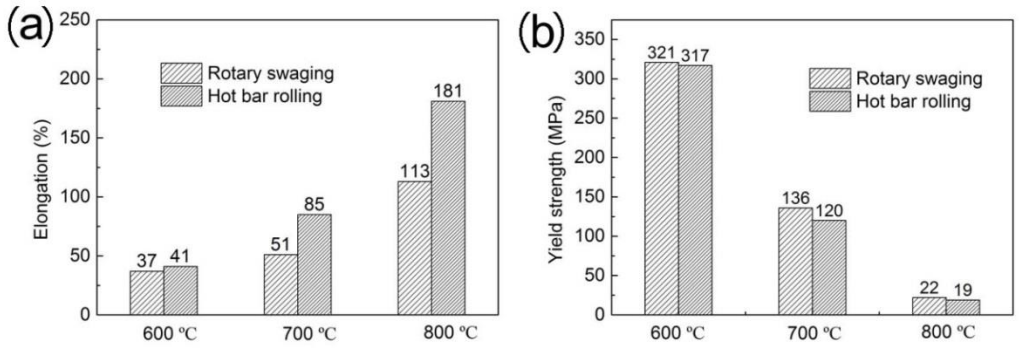

Figure 12. (a) elongation and (b) yield stress for both the rotary swaged and hot rolled bars of Fe-6.5wt.% Si alloy at various tensile temperatures.

Based on the design of the hot bar rolling technology and on the analysis of microstructures, textures, ordered structures, and mechanical property, the Fe-6.5wt.% Si bars with fine equiaxed grain were successfully fabricated. With the absence of DO_3 ordered phase and the fine grain in the as bar rolled sample, a higher ductility of the as hot rolled bar can be obtained, compared with the rotary swaged bar. The hot bar rolling is a better method to fabricate the Fe-6.5wt.% Si bars to improve the processing efficiency of the Fe-6.5wt.% Si wires.

5. Conclusions

The hot bar rolling parameters of the Fe-6.5wt.% Si alloy were designed. The evolutions of the microstructure, texture and ordered structure were investigated, and the mechanical property of the Fe-6.5wt.% Si bars was studied. The following conclusions can be drawn:

(1) The Φ7.5 mm Fe-6.5wt.% Si bars with fine equiaxed grain were successfully fabricated through three rolling stages: rough rolling (hexagon-square-oval-square) at 850–900 °C, medium rolling (oval-square-oval-round) at 800–850 °C, and finish rolling (oval-square-oval-round) at 800–850 °C.

(2) During the hot bar rolling, the area fractions of the {100}<011> oriented grains and the {011}<100> oriented grains decreased to 0, however, the {100}<001> component, the {011}<211> component and the {112}<110> component increased. Notably, γ fiber with {111}<110> component was dominant.

(3) DO_3 ordered phase were suppressed, and the B2 ordered domains were refined, leading to the decrease of ordering degree after the hot bar rolling. Higher ductility of the hot rolled bar was obtained, compared with the rotary swaged bar. Hence, the hot bar rolling technology is the excellent process to fabricate the Fe-6.5wt.% Si bars.

Acknowledgments: Financial supports from the Natural Science Foundation of China (51471031, U1660115) and the State Key Laboratory for Advanced Metals and Materials (2016Z-17) are gratefully acknowledged.

Author Contributions: Shibo Wen conceived, designed, performed the experiments and wrote the manuscript; Shaowei Xue, Chaoyu Han and Binbin Liu contributed to some experiments such as the EBSD and the hot bar rolling; Yongfeng Liang and Feng Ye supervised the work.

Conflicts of Interest: The authors declare no conflict of interest.

References

1. Arai, K.; Tsuya, N. Ribbon-form silicon-iron alloy containing around 6.5 percent silicon. *IEEE. Trans. Magn.* **1980**, 16, 126-129, 10.1109/TMAG.1980.1060560.
2. Narita, K.; Teshima, N.; Mori, Y.; Enokizono. M. Recent researches on high silicon-iron alloys. *IEEE. Trans. Magn.* **1981**, 17, 2857-2862, 10.1109/TMAG.1981.1061740.

3. Raviprasad, K.; Tenwick, M.; Davies, H.A.; Chattopadhyay, K. The nature of ordered structures in melt spun iron-silicon alloys. *Scripta. Mater.* **1986**, 20, 1265-1270, 10.1016/0036-9748(86)90045-1.
4. Raviprasad, K.; Chattopadhyay, K. The influence of critical points and structure and microstructural evolution in iron rich Fe-Si alloys. *Acta. Metall.* **1993**, 41, 609-624, 10.1016/0956-7151(93)90091-6.
5. Takada, Y.; Abe, M.; Masuda, S.; Inagaki, J. Commercial scale production of Fe-6.5wt.% Si sheet and its magnetic properties. *J. Appl. Phys.* **1988**, 64, 5367-5369, 10.1063/1.342373.
6. Ros-Yanez, T.; Houbaert, Y.; Gómez Rodríguez, V. High-silicon steel produced by hot dipping and diffusion annealing. *J. Appl. Phys.* **2002**, 91, 7857-7859, 10.1063/1.1449445.
7. He, X.D.; Li, X.; Sun, Y. Microstructure and magnetic properties of high silicon electrical steel produced by electron beam physical vapor deposition. *J. Magn. Magn. Mater.* **2008**, 320, 217-221, 10.1016/j.jmmm.2007.05.030.
8. Machado, R.; Kasama, A.H.; Jorge, A.M.; Kiminami, C.S.; Botta Fo, W.J.; Bolfarini, C. Evolution of the texture of spray-formed Fe-6.5wt.%Si-1.0wt.%Al alloy during warm-rolling. *Mater. Sci. Eng. A.* **2007**, 449-451, 854-857, 10.1016/j.msea.2006.03.132..
9. Lima, C.C.; Da Silva, M.C.A.; Sobral, M.D.C.; Coelho, R.E.; Bolfarini, C. Effects of order–disorder reactions on rapidly quenched Fe-6.5%Si alloy. *J. Alloys. Compd.* **2014**, 586, S314-S316, 10.1016/j.jallcom.2012.09.074.
10. Fish, G.E.; Chang, C.F.; Bye, R. Frequency dependence of core loss in rapidly quenched Fe-6.5 wt.% Si. *J. Appl. Phys.* **1988**, 64, 5370-5372, 10.1063/1.342374.
11. Liang, Y.F.; Wang, S.; Li, H.; Jiang, Y.M.; Ye, F. Fabrication of Fe-6.5wt%Si ribbons by melt spinning method on large scale. *Adv. Mater. Sci. Eng.* **2015**, 1-5, 10.1155/2015/296197.
12. Wang, S.; Jiang, Y.M.; Liang, Y.F.; Ye, F.; Lin, J.P. Magnetic properties and core loss behavior of Fe-6.5wt.%Si ribbons prepared by melt spinning. *Adv. Mater. Sci. Eng.* **2015**, 1-6, 10.1155/2015/410830.
13. Li, R.; Shen, Q.; Zhang, L.; Zhang, T. Magnetic properties of high silicon iron sheet fabricated by direct powder rolling. *J. Magn. Magn. Mater.* **2004**, 281, 135-139, 10.1016/j.jmmm.2004.04.098.
14. Liang, Y.F.; Ye, F.; Lin, J.P.; Wang, Y.L.; Chen, G.L. Effect of annealing temperature on magnetic properties of cold rolled high silicon steel thin sheet. *J. Alloys. Compd.* **2010**, 491, 268-270, 10.1016/j.jallcom.2009.10.118.
15. Patterson, E.E.; Field, D.P.; Zhang, Y. Characterization of twin boundaries in an Fe-17.5Mn-0.56C twinning induced plasticity steel. *Mater. Charact.* **2013**, 85, 100-110, 10.1016/j.matchar.2013.08.016.
16. Liang, Y.F.; Ye, F.; Lin, J.P.; Wang, Y.L.; Zhang, L.Q.; Chen, G.L. Effect of heat treatment on mechanical properties of heavily cold-rolled Fe-6.5wt.%Si alloy sheet. *Sci. China Technol. Sci.* **2010**, 53, 1008-1011, 10.1007/s11431-010-0125-1.
17. Di Giulio, M. Transformer with magnetic core of coiled wires. Brazil, 2000, WO 00/44006.
18. Yang, W.; Li, H.; Yang, K.; Liang, Y.F.; Yang, J.; Ye, F. Hot drawn Fe-6.5wt.%Si wires with good ductility. *Mater. Sci. Eng. B.* **2014**, 186, 79-82, 10.1016/j.mseb.2014.03.013.
19. Lee, Y. Rod and bar rolling: theory and applications , CRC Press, America, 2004, 9780824756499.
20. Liang, Y.F.; Lin, J.P.; Ye, F.; Li, Y.J.; Wang, Y.L.; Chen, G.L. Microstructure and mechanical properties of rapidly quenched Fe-6.5wt.% Si alloy. *J. Alloys. Compd.* **2010**, 504, S476-S479, 1016/j.jallcom.2010.03.075.
21. Cheng, Z.Y.; Liu, J.; Zhu, J.C.; Xiang, Z.D.; Jia, J.; Bi, Y.J. Microstructure, texture evolution and magnetic properties of Fe-6.5wt.%Si and Fe-6.5wt.%Si-0.5wt.%Cu alloys during rolling and annealing treatment. *Metals*. **2018**, 8, 144, 10.3390/met8020144.
22. Machado, R.; Kasama, A.H.; Jorge, A.M.; Kiminami, C.S.; Botta Fo, W.J.; Bolfarini, C. Evolution of the texture of spray-formed Fe-6.5wt.% Si-1.0wt.% Al alloy during warm-rolling. *Mater. Sci. Eng. A.* **2007**, 449-451, 854-857, 10.1016/j.msea.2006.03.132.
23. Said, A.; Lenard, J.G.; Ragab, A.R.; Elkhier, M.A. The temperature, roll force and roll torque during hot bar rolling. *J. Mater. Process. Tech.* **1999**, 88, 147-153, 10.1016/S0924-0136(98)00391-4.
24. Kwon, H.C.; Im, Y.T. Interactive computer-aided-design system for roll pass and profile design in bar rolling. *J. Mater. Process. Tech.* **2002**, 123, 399-405, 10.1016/S0924-0136(02)00100-0.
25. Song, R.B. The technology of rolling, Metallurgical Industry Press, China, 2014, 978-7-5024-6506-3.
26. Wen, S.B.; Han, C.Y.; Zhang, B.; Liang, Y.F.; Ye, F.; Lin, J.P. Flow behavior characteristics and processing map of Fe-6.5wt.%Si alloys during hot compression. *Metals*. **2018**, 8, 186, 10.3390/met8030186.
27. Zhang, H.; Li, H.; Yang, K.; Liang, Y.F.; Ye, F. Optimization of heat treatment process of Fe-6.5%Si sheet. *Acta. Metall. Sin.* **2013**, 49, 1445-1451, 10.3724/SP.J.1037.2013.00520.
28. Hölscher, M.; Raabe, D.; Lücke, K. Relationship between rolling textures and shear textures in fcc and bcc metals. *Acta. Mater.* **1994**, 42, 879-886, 10.1016/0956-7151(94)90283-6.

29. Dillamore, I.L.; Roberts, W.T. Rolling textures in fcc and bcc metals. *Acta. Mater.* **1964**, 12, 281-293, 10.1016/0001-6160(64)90204-4.
30. Dong, N.L. The evolution of recrystallization textures from deformation textures. *Scripta. Mater.* **1994**, 32, 1689-1694, 10.1016/0956-716X(95)00256-U.
31. Li, K.; Yang, P. The formation of strong {100} texture by dynamic strain-induced boundary migration in hot compressed Ti-5Al-5Mo-5V-1Cr-1Fe alloy. *Metals*. **2017**, 7, 412, 10.3390/met7100412.
32. Marcinkowski, M.J.; Brown, N. Direct observation of antiphase boundaries in the Fe_3Al superlattice. *J. Appl. Phys.* **1962**, 33, 537-552, 10.1063/1.1702463.
33. Yu, J.H.; Shin, J.S.; Bae, J.S.; Lee, Z.H.; Lee, T.D. The effect of heat treatments and Si contents on B2 ordering reaction in high-silicon steels. *Mater. Sci. Eng. A*. **2001**, 307, 29-34, 10.1016/S0921-5093(00)01960-2.
34. Jung, H.; Kim, J. Influence of cooling rate on iron loss behavior in 6.5wt% grain-oriented silicon steel. *J. Magn. Magn. Mater*. **2014**, 353, 76-81, 10.1016/j.jmmm.2013.10.004.
35. Li, H.; Liang, Y.F.; Yang, W.; Ye, F.; Lin, J.P.; Xie, J.X. Disordering induced work softening of Fe-6.5wt%Si alloy during warm deformation. *Mater. Sci. Eng. A*. **2015**, 628, 262-268, 10.1016/j.msea.2015.01.058.
36. Callister Jr, W.D.; Rethwisch, D.G. Fundamentals of materials science and engineering: an integrated approach, John Wiley and Sons, America, 2012, 0-471-39551-X.
37. Yang, W. Fabrication and properties of wires of Fe-6.5%Si electrical steel. M.S. Thesis, Uni. Sci. Tech. Beijing, Beijing, 2013.
38. Li, H.; Liang, Y.F.; Ye, F. Effect of heat treatment on ordered structures and mechanical properties of Fe-6.5mass%Si alloy. *Mater. Trans.* **2015**, 56, 759-765, 10.2320/matertrans.M2014451.